Calibrated Si Mobility and Incomplete Ionization Models with Field Dependent Ionization Energy for Cryogenic Simulations

Hiu Yung Wong
Electrical Engineering
San Jose State University
San Jose, USA
hiuyung.wong@sjsu.edu

***Abstract*— Cryogenic silicon CMOS operating between 77K and 4.2K is becoming more popular in high-speed server applications and the periphery of quantum computers. In the cryogenic regime, dopant incomplete ionization and field enhanced ionization become dominating physical phenomena. Therefore, it is important to use accurate and well-calibrated mobility and incomplete ionization models in cryogenic TCAD simulations. In this paper, we present a Philips Unified Mobility Model (PhuMob) and Altermatt's incomplete ionization model calibrated between 300K and 20K for boron and arsenic dopants in silicon across 5 orders of magnitude in doping concentration. A novel method is proposed to include field-dependent ionization energy in Altermatt's model, which results in good convergence even in 3D TCAD simulations at 4K.**

Keywords—Cryogenic, Field Dependent Ionization, Incomplete Ionization, TCAD

I. Introduction

Cryogenic electronics operating between 77K (the boiling point of liquid-nitrogen) and 4.2K (the boiling point of liquid-helium) are attracting considerable attention due to the emergence of quantum computers [1][2], the quest for higher performance servers for big data processing using existing technologies [3], and the revival of deep space exploration [4][5]. For example, cryogenic CMOS devices are indispensable for the control and readout circuits in quantum computers. To provide low latency, CMOS circuits need to be in close proximity to the qubits and thus need to operate at cryogenic temperatures [1][2]. Cryo-CMOS also delivers improved performance in terms of on-state/leakage current ratio, subthreshold swing, and transconductance and is expected to improve the high-performance servers substantially [6][7]. In space applications, temperatures can drop to 44K on the surface of Pluto, or 3K in interstellar space [5].

TCAD has been the powerhouse technique for semiconductor device development in the last few decades [8]. However, TCAD is not ready to be fully deployed for cryogenic CMOS development. Firstly, cryogenic physics models and parameters have not been fully understood (e.g. subthreshold swing, [9]), developed, and calibrated for effective TCAD simulation. Secondly, numeric convergence is challenging in low-temperature TCAD simulation due to the vanishingly small intrinsic carrier concentration [10]. Even with simple models, convergence is still very difficult below 15K [11].

In this paper, we self-consistently calibrated some of the most important cryogenic CMOS models, namely the incomplete ionization model for Boron and Arsenic and low-field carrier (both hole and electron) mobility models from 300K to 20K based on experimental data [12]. A new method of simulating incomplete ionization is also proposed which achieves excellent convergence at 4K even for 3D simulations that include field-dependent ionization.

II. Model Selection

At cryogenic temperatures, dopants are not fully ionized due to their finite ionization energies (E_A). However, when the doping concentration is high, impurity bands are formed (Mott transition [13][14]) (Fig. 1). Moreover, E_A is a function of doping concentration and given by the following equation in [13] and [14],

$$E_A = \frac{E_{A0}}{1 + \left(\frac{N_{dop}}{N_{ref}}\right)^c} \qquad (1)$$

where E_{A0} is the ionization energy of isolated dopants in the absence of field enhancement, N_{dop} is the dopant concentration, and N_{ref} and c are fitting parameters. N_{ref} can be regarded as the doping concentration above which E_A is significantly reduced.

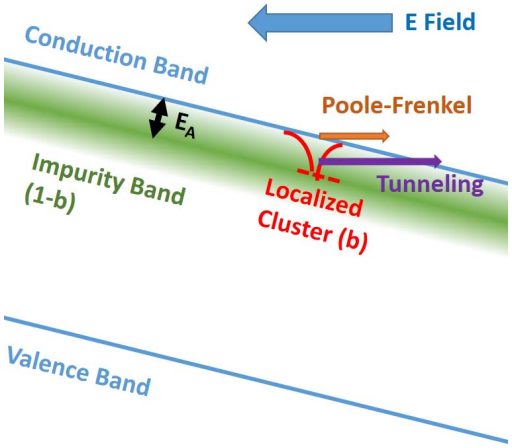

Figure 1: Illustration of n-type dopant ionization in Silicon. Impurity band just merging with the conduction band is illustrated. While all donor electrons in the impurity band (fraction (*1-b*) of total) can contribute to the electrical conduction, the fraction *b* of the donor electrons can only contribute to electrical conduction through ionization. The effective ionization energy E_A depends on doping concentration and can be lower when Poole-Frenkel or tunneling effects are strong.

According to [13][14], there are two sources of free carriers contributing to the conduction current. One is localized states (including localized dopant clusters) whose carriers are thermally ionized into the conduction band. Their ionization rate depends on E_A, temperature, and electric field. Another is the delocalized carriers (e.g. those residing in the impurity bands). The fraction of the delocalized carriers is given by the following equation ([13] and [14]),

$$b = \frac{1}{1 + \left(\frac{N_{dop}}{N_b}\right)^d} \qquad (2)$$

where N_b and d are fitting parameters. N_b can be regarded as the doping concentration above which clusters merge to form the impurity band at the expense of isolated carriers or clusters.

In [13][14], an equation was derived for TCAD simulations and calibrated at 300K to account for these effects (dubbed Altermatt's model). We implemented this model using the Physical Model Interface (PMI) in Sentaurus Device [15] and calibrated to experimental data from the literature [12] down to cryogenic temperatures. Reference [12] is relatively old. The experimental data accuracy may not be as high as desired (in particular, the compensation doping concentration). However, it has the most extensive data in terms of doping concentration and temperature ranges available in the literature.

To model the carrier mobility at cryogenic temperature, we need to take into account that dopants are not fully ionized and thus the impurity scattering is reduced. Moreover, screening of ionized impurities by carriers should also be included for accurate simulations. Philips Unified Mobility Model (PhuMob) [16] is chosen because it includes carrier screening and temperature effects.

Under high electric field, the effective dopant ionization energy is reduced due to tunneling and Poole Frenkel ionization [17]. This will greatly affect the dopant ionization behavior and should be considered in TCAD simulations at cryogenic temperatures.

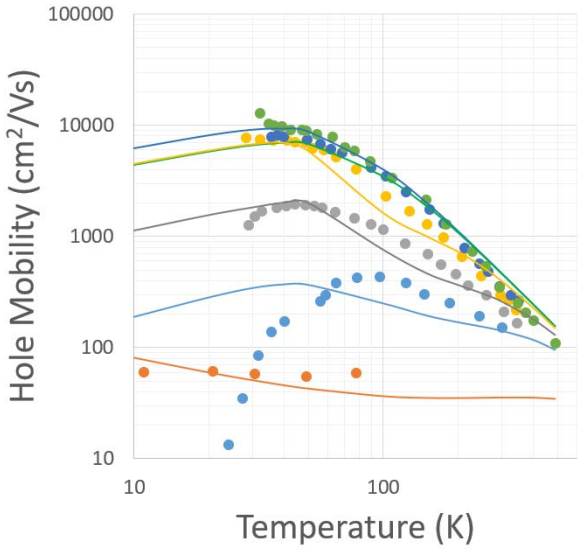

Figure 3: Hole mobility as a function of temperature and boron concentration. Markers: experimental data in [12]. Lines: TCAD simulation. Net impurity concentrations from *bottom to top* are 1.5×10^{19}cm^{-3}, 10^{18}cm^{-3}, 2×10^{17}cm^{-3}, 2.4×10^{16}cm^{-3}, 7×10^{14}cm^{-3} and 3.1×10^{14}cm^{-3}, respectively.

III. Calibration of Ionization and Mobility Models

Due to the interplay between the aforementioned physics, it is important to calibrate carrier concentrations and mobilities self-consistently as carrier mobility depends strongly on ionized dopant concentration at low temperatures. Boron and arsenic doped silicon data at various doping concentrations and temperatures from [12] are used for calibrations. Fig. 2 to Fig. 5 show the calibrated free carrier concentrations and their mobilities using PhuMob and Altermatt's models. It should be noted that there may be some

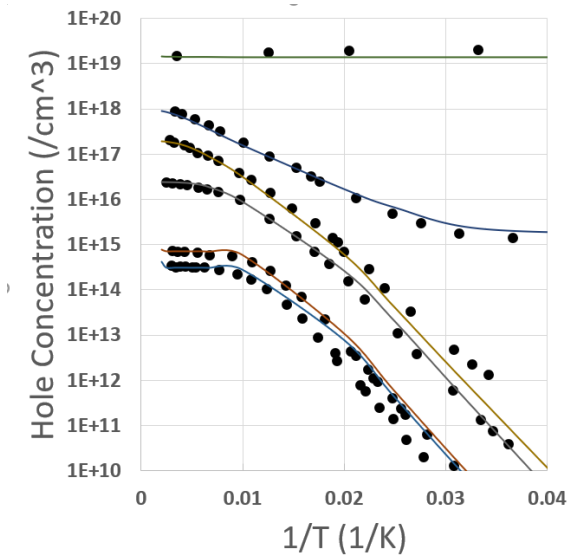

Figure 2: Free hole concentration as a function of temperature and boron concentration. Markers: experimental data in [12]. Lines: TCAD simulation. Net impurity concentrations from top to bottom are 1.5×10^{19}cm^{-3}, 10^{18}cm^{-3}, 2×10^{17}cm^{-3}, 2.4×10^{16}cm^{-3}, 7×10^{14}cm^{-3} and 3.1×10^{14}cm^{-3}, respectively.

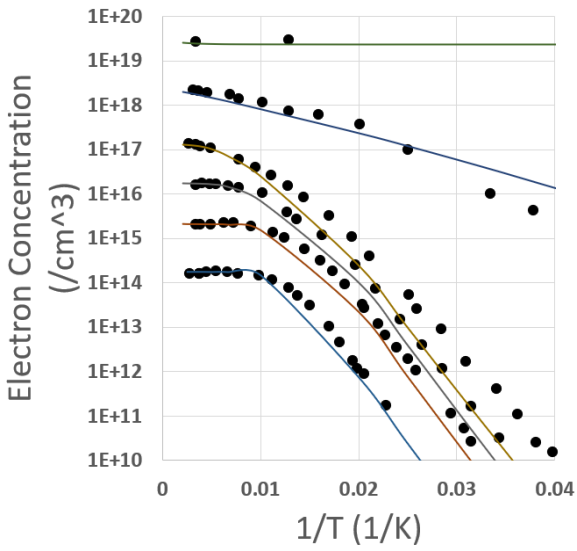

Figure 4: Free electron concentration as a function of temperature and arsenic concentration. Markers: experimental data in [12]. Lines: TCAD simulation. Net impurity concentrations from top to bottom are 2.7×10^{19}cm^{-3}, 2.2×10^{18}cm^{-3}, 1.3×10^{17}cm^{-3}, 1.75×10^{16}cm^{-3}, 2.1×10^{15}cm^{-3} and 1.75×10^{14}cm^{-3}, respectively.

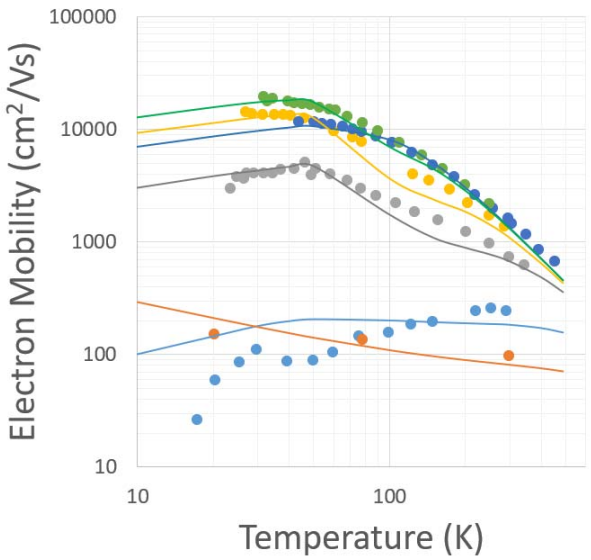

Figure 5: Electron mobility as a function of temperature and boron concentration. Markers: experimental data in [12]. Lines: TCAD simulation. Net impurity concentrations from *bottom to top* are 2.7×10^{19}cm^{-3}, 2.2×10^{18}cm^{-3}, 1.3×10^{17}cm^{-3}, 1.75×10^{16}cm^{-3}, 2.1×10^{15}cm^{-3} and 1.75×10^{14}cm^{-3}, respectively

measurement errors in reference [12] especially due to the uncertainty of compensation doping levels. Reference [12] also mentions that a few of their low-temperature mobility data points are anomalous. Therefore, it is difficult to obtain a perfect fit to their data. However, with a single set of parameters, we are able to obtain good overall fittings between 300K and 20K for doping concentrations from 10^{14}cm^{-3} to 10^{19}cm^{-3}.

The fitting is obtained by using the default parameters with the following modifications. In Altermatt's model [14], N_b is 3.6×10^{18}cm^{-3} instead of 6×10^{18}cm^{-3} for boron (Equation 2). N_{ref} is 10^{18}cm^{-3} instead of 4×10^{18}cm^{-3} for Arsenic (Equation 1). These modifications are important to fit the intermediate doping level curves ($10^{17}\sim10^{18}$cm^{-3}).

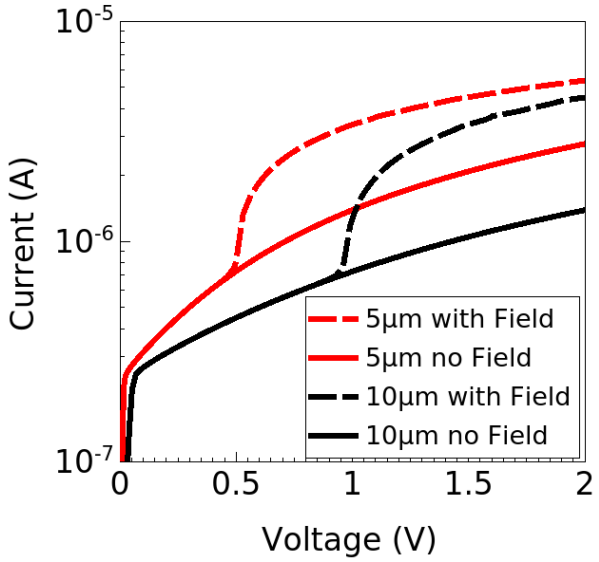

Figure 6: IV curves of 3D resistors of various lengths with and without field dependent model turned on.

In the PhuMob model, the default parameters are kept unchanged as much as possible. The major modification is changing the μ_{min} of Boron to 14cm^2/V·s instead of 44.9cm^2/V·s [15][16]. It is also important to adjust the compensation dopant concentration to obtain good fitting of the mobility curves at low temperatures in the low dopant concentration samples. This is because at low temperatures, dopants are mostly not ionized and the compensation dopants contribute strongly to the scattering effect. Compensation doping concentrations are chosen based on [12] with reasonable adjustments. It should also be noted that each curve in Fig. 2 to 5 corresponds to a certain *net impurity* concentration, which is the difference between the dopant concentration and the compensation dopant concentration. The compensation dopant concentrations used in the fittings are given in Table I.

TABLE I. COMPENSATION DOPING IN FIG. 2 TO FIG. 5

p-type (cm^{-3})[a]		n-type (cm^{-3})[a]	
Experiment	TCAD	Experiment	TCAD
4.1×10^{14}	3.1×10^{14}	1.0×10^{14}	8.0×10^{14}
2.2×10^{14}	5.2×10^{14}	5.25×10^{14}	3.0×10^{14}
2.3×10^{15}	5.0×10^{15}	1.48×10^{15}	5.0×10^{14}
4.9×10^{15}	4.0×10^{15}	2.2×10^{15}	3×10^{15}
Unknown	5.0×10^{16}	Unknown	5×10^{17}
Unknown	2.9×10^{15}	Unknown	5×10^{17}

[a] Each row corresponds to each curve in Figs. 2 to 4 with increasing net impurity concentration from top to bottom

IV. SIMULATION WITH FIELD DEPENDENT IONIZATION

To include field-dependent ionization in Altermatt's model, one may modify equation (1) by including field-dependent terms. However, the incomplete ionization PMI used converges very poorly when field-dependent effects are included because the PMI is not designed for this purpose (e.g. lack of Jacobian for electric field). To improve convergence, we propose to model the delocalized dopant states as conventional dopants not subject to incomplete ionization (i.e. all of these dopants are ionized and they are a fraction (1-b) of the total dopants). The localized dopant states are modeled using traps with the same final E_A given by Altermatt's model that are a fraction b of the total dopants (Fig. 1). The partition between these two types of dopants is calculated using Altermatt's model (i.e. Equation (2)) and the calibrated Altermatt parameters are used. The Trap Energy Shift PMI [15] is then employed to include the field-dependent effect on E_A. This is dubbed "*b-method*".

This model is applied to 3D resistors of various lengths (L) doped with 10^{14} cm^{-3} arsenic at 4K sandwiched by two regions with fully ionized dopants of about 10nm length. The short fully ionized regions are contacted with Ohmic contact boundaries. Altermatt's model is included using the proposed method. The calibrated PhuMob model and ionization energy lowering due to the Poole-Frenkel effect are also incorporated. The field dependency is set up such that significant E_A reduction occurs when the electric field is about 0.1V/µm [17]. Fig. 6 shows the IV curves of L = 5 µm and 10 µm. It

can be seen that when the electric field is less than the critical field (0.5V for 5 µm and 1V for 10 µm), without and without field ionization the model give the same results. Once the critical electric field is reached, field ionization increases the current substantially.

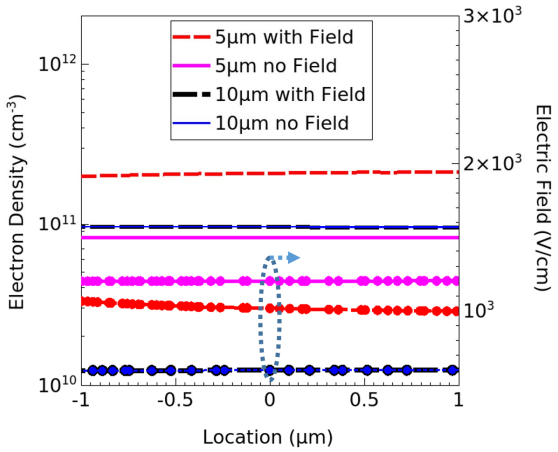

Figure 7: Electron density and electric field profiles along the resistors in Fig. 6 in the transport direction when V = 0.6V. The midpoint of the resistor is at 0µm. Curves with markers are electric field. The two 10 µm curves overlap with each other.

Fig. 7 shows the electron density and electric field plots along the transport direction of the resistors at V = 0.6V. Since the electric field is still below the critical field in the L = 10 µm case, with and without field dependent ionization give the same result. For L = 5 µm, with field dependence has higher current density. Note that it also has lower field because it is more conductive.

It is well-known that convergence in TCAD simulations is problematic at cryogenic temperatures. It typically becomes more problematic when including the impact of field dependent ionization. With the proposed method the convergence is excellent. Although not shown, good convergence is also achieved for transistor simulations at 4K.

V. Conclusions

An incomplete ionization model (Altermatt's model) and mobility model (PhuMob) are calibrated to experimental data from 300K to 20K for a wide range of doping concentrations (10^{14}cm^{-3} to 10^{19}cm^{-3}) for boron and arsenic doped silicon. Resulting simulations capture important features such as the plateau in free carrier curves at medium doping levels.

A new method is also proposed to perform effective TCAD simulations at cryogenic temperature in which field-dependent ionization is included in the Altermatt's model. It shows excellent convergence in a 3D resistor simulation at 4K.

Acknowledgment

The author thanks Dr. Gibson for his suggestion of *b-method* to improve convergence.

References

[1] E. Charbon, F. Sebastiano, A. Vladimirescu, H. Homulle, S. Visser, L. Song, and R M. Incandela, "Cryo-CMOS for Quantum Computing," 2016 IEEE International Electron Devices Meeting (IEDM), San Francisco, CA, 2016, pp. 13.5.1-13.5.4, doi: 10.1109/IEDM.2016.7838410.

[2] M. J. Gong, U. Alakusu, S. Bonen, M. S. Dadash, L. Lucci, H. Jia, et al., "Design Considerations for Spin Readout Amplifiers in Monolithically Integrated Semiconductor Quantum Processors," 2019 IEEE Radio Frequency Integrated Circuits Symposium (RFIC), Boston, MA, USA, 2019, pp. 111-114, doi: 10.1109/RFIC.2019.8701847.

[3] G. Lee, D. Min, I. Byun and J. Kim, "Cryogenic computer architecture modeling with memory-side case studies," 2019 ACM/IEEE 46th Annual International Symposium on Computer Architecture (ISCA), Phoenix, AZ, USA, 2019, pp. 774-787.

[4] D. Clery, "U.S. lawmaker orders NASA to plan for trip to Alpha Centauri by 100th anniversary of moon landing," Science, May 23, 2016 [Online]. DOI: 10.1126/science.aag0558

[5] R. L. Patterson, A. Hammoud, J. E. Dickman, S. Gerber, M. Elbuluk and E. Overton, "Electronics for Deep Space Cryogenic Applications," Proceedings of the 5th European Workshop on Low Temperature Electronics, Grenoble, France, 2002, pp. 207-210, doi: 10.1109/WOLTE.2002.1022482.

[6] A. Beckers, F. Jazaeri and C. Enz, "Cryogenic MOS Transistor Model," in IEEE Transactions on Electron Devices, vol. 65, no. 9, pp. 3617-3625, Sept. 2018, doi: 10.1109/TED.2018.2854701.

[7] H. Homulle, F. Sebastiano and E. Charbon, "Deep-Cryogenic Voltage References in 40-nm CMOS," IEEE Solid-State Circuits Letters, vol. 1, no. 5, pp. 110-113, May 2018, doi: 10.1109/LSSC.2018.2875821.

[8] R. Minixhofer, "TCAD as an Integral Part of the Semiconductor Manufacturing Environment," 2006 International Conference on Simulation of Semiconductor Processes and Devices, Monterey, CA, 2006, pp. 9-16, doi: 10.1109/SISPAD.2006.282827.

[9] A. Beckers, F. Jazaeri and C. Enz, "Revised Theoretical Limit of Subthreshold Swing in Field-effect Transistors," arXiv:1811.09146, 2019.

[10] L. Luo, "Physics, Compact Modeling and TCAD of SiGe HBT for Wide Temperature Range Operation," Ph.D. dissertation, ECE, Auburn University, Auburn, AL, 2011.

[11] F. A. Mohiyaddin, F. G. Curtis, M. N. Ericson and T. S. Humble, "Simulation of Silicon Nanodevices at Cryogenic Temperatures for Quantum Computing," Proceedings of the 2017 COMSOL Conference in Boston.

[12] F. J. Morin and J. P. Maita, "Electrical properties of silicon containing arsenic and boron," Phys. Rev. 96, 28, 1954.

[13] P. P. Altermatt, A. Schenk and G. Heiser, "A Simulation model for the density of states and for incomplete ionization in crystalline Silicon. I. stablishing the model in Si:P," Journal of Applied Physics, vol. 100, 113714 (2006).

[14] P. P. Altermatt, A. Schenk, B. Schmithüsen and G. Heiser, "A simulation model for the density of states and for incomplete ionization in crystalline silicon. II. Investigation of Si:As and Si:B and usage in device simulation," Journal of Applied Physics, vol. 100, 113715 (2006).

[15] Sentaurus™ Device User Guide Version Q-2019.12, December 2019.

[16] D. B. M. Klaassen, "A unified mobility model for device simulation—I. Model equations and concentration dependence," Solid-State Electronics, Vol. 35, No. 7, pp.953-959, 1992.

[17] D. P .Forty, "Impurity ionization in MOSFETs at very low temperatures," Cryogenics, Volume 30, Issue 12, December 1990, Pages 1056-1063.